Band-edge diagrams for strained III–V semiconductor quantum wells, wires, and dots

C. E. Pryor*
Department of Physics and Astronomy, University of Iowa, Iowa City, Iowa 52242, USA

M.-E. Pistol†
Solid State Physics, Lund University, P.O. Box 118, SE-221 00 Lund, Sweden
(Received 20 October 2004; revised manuscript received 19 July 2005; published 8 November 2005)

We have calculated band-edge energies for most combinations of zinc blende AlN, GaN, InN, GaP, GaAs, InP, InAs, GaSb, and InSb in which one material is strained to the other. Calculations were done for three different geometries (quantum wells, wires, and dots) and mean effective masses were computed in order to estimate confinement energies. For quantum wells, we have also calculated band-edges for ternary alloys. Energy gaps, including confinement, may be easily and accurately estimated using band energies and a simple effective mass approximation, yielding excellent agreement with experimental results. By calculating all material combinations we have identified interesting material combinations, such as artificial donors, that have not been experimentally realized. The calculations were perfomed using strain-dependent $\mathbf{k}\cdot\mathbf{p}$ theory and provide a comprehensive overview of band structures for strained heterostructures.

DOI: 10.1103/PhysRevB.72.205311 PACS number(s): 73.22.−f, 78.67.Hc, 78.67.Lt, 78.67.De

I. INTRODUCTION

Diagrams of band edges versus material composition or lattice constant for bulk semiconductors[1] have proved indispensable for band-gap engineering. For heterostructures containing materials with two different lattice constants, however, such diagrams are problematic because the band energies are modified by strain. A familiar example is the band gap of InAs ($E_g \approx 0.41$ eV) which approximately doubles when grown on GaAs. The strain depends on the lattice mismatch, the elastic properties of both materials, and the geometry. The energy shift in turn depends on the strain and the electronic material parameters, primarily the deformation potentials. Theoretical treatments often rely on approximating a structure as a slab because it is amenable to simple analytic calculations, in spite of the fact that wires and dots are poorly approximated by a slab, particularly in their strain distribution.

To address this problem, we have calculated strain-dependent band energies for heterostructures consisting of direct gap binary III-V compounds, including zinc-blende nitrides, and also including GaP and AlN as substrate materials. We have taken the geometries of the embedded materials to be (001)-oriented slabs (quantum wells), circular wires oriented along [001], and lens-shaped dots. We have restricted ourselves to direct gap materials because they are the most interesting for optical applications, and because deformation potentials for indirect materials are less well known. For quantum wells we have also calculated band energies for ternary alloys grown on substrates having lattice constants between 5.4 and 6.5 nm. The results provide a systematic and comprehensive resource for the design and interpretation of strained low-dimensional heterostructures.

For some material combinations the extremely large lattice mismatch makes the growth of pseudomorphic structures on large area substrates problematic. However, there has been progress in the fabrication of heterostructures in free-standing wires or whiskers[2] with diameters between 10 and 100 nm. Whiskers allow the realization of larger mismatches in part because relaxation of the barrier material results in smaller strain in the well material. The lack of misfit dislocations in whiskers may allow heterostructures to be grown beyond the classical limit of Matthews and Blakeslee.[3] While we do not consider such wires here, the results for slabs are applicable.

In Sec. II we describe the method for computing strain, electronic energies, effective masses, and estimating confinement energies. In Sec. III we present results for slabs, wires, and dots composed of binary materials and compare with available experiments. In Sec. IV we present mean effective masses for structured composed binary alloys. In Sec. V we consider slabs of ternary alloys of varying composition on substrates of binary materials.

II. METHOD

The calculations were performed by a method that has been previously described.[4,5] The strain was calculated using continuum elasticity and the finite element method. Spatially dependent energies were then computed using the local value of the strain with an eight-band strain-dependent $\mathbf{k}\cdot\mathbf{p}$ Hamiltonian[6] for $\mathbf{k}=0$. Since the valence and conduction bands are coupled by terms proportional to $\mathbf{k}$, the band energies are, in fact, computed using a $6+2$ band model, however the effective mass calculations make use of the full eight-band model.

All material parameters were taken from Ref. 7 with $T=0$ K, and all nitrides were taken to be in the zinc-blende form. The final results depend on the material parameters of each semiconductor, including the lattice constant, elastic constants, unstrained valence band energy, energy gap, spin-orbit coupling, Luttinger parameters (for effective masses), Kane momentum matrix element (for effective masses), deformation potentials, and bowing parameters (where avail-

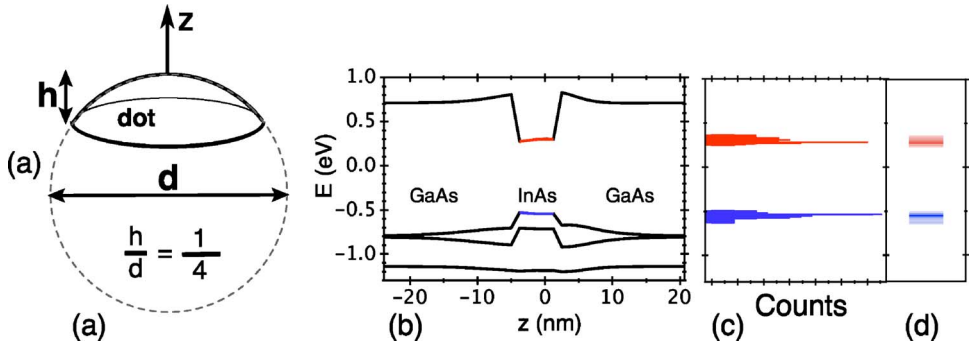

FIG. 1. (Color online) (a) The lens-shaped geometry used for all quantum dot calculations. The dot height is $\frac{1}{4}$ the diameter of sphere out of which the lens is cut. The z-axis is along [001]. (b) Band structure as a function of position along an InAs/GaAs dot's axis of symmetry. The energies are calculated for $k=0$ using the local value of the strain. (c) Histogram of the conduction and valence band edges including each point in the dot. (d) Histogram as a shaded density, as shown in Figs. 3–10.

able). Material parameters are subject to varying degrees of uncertainty, and the calculations presented here are primarily constrained by the accuracy of these tabulated parameters. The parameters for the nitrides are especially uncertain, and mostly based on theoretical calculations. For example, the band gap of wurtzite InN has recently been reevaluated by a large factor.[8] Previous investigations have shown that calculations for strained heterostructures vary in their sensitivity to material parameters, with the deformation potentials and Luttinger parameters being the most important.[9] Even for well characterized materials the parameters are known with varying degrees of accuracy. For example, lattice and elastic constants are known to four or more significant figures, while Luttinger parameters are typically only certain to within a few tens of percent.

The computational grids were $100\times100\times100$ and 100×100 for dots and wires, respectively. For wells only two sites were needed since the strain is biaxially symmetric. As a check on the results, the calculations were done independently by each author. For wires and dots the independent calculations were done with the same software, but the quantum well calculations were checked by using different programs.

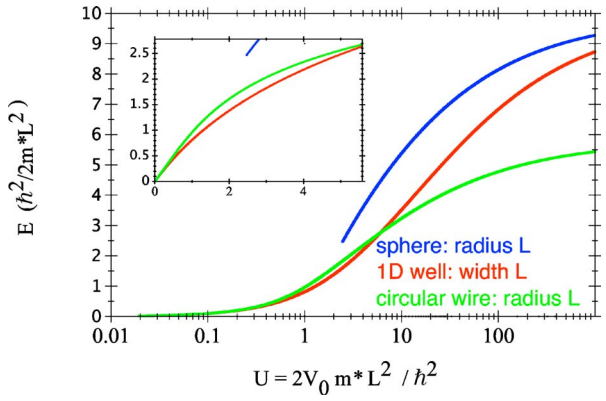

FIG. 2. (Color online) Confinement energy as a function of the barrier height V_0, the effective mass m^* (in the well and barrier material), and the dimension of the structure, L. For $V_0=1$ eV, $m^*=m_e$, and $L=1$ nm, $U=26.247$. There is always a bound state for the 1D and 2D cases, but for 3D a minimum potential strength is required.

For bulk materials the band edges are characterized by single numbers, as are the band edges for strained quantum wells since their strain is homogeneous. For wires and dots, however, the inhomgeneity of the strain gives rise to spatial variation in the band edge (Fig. 1). To represent complex strain distributions, histograms of the band edges were computed.

While a band edge is well-defined for bulk materials, wires, and wells, quantum dots do not have bands. Nonetheless, it is useful to consider the local band edge that would be present in bulk material having the same strain as a location in the heterostructure. For a sufficiently large heterostructure such band edges give the potential in the effective mass ap-

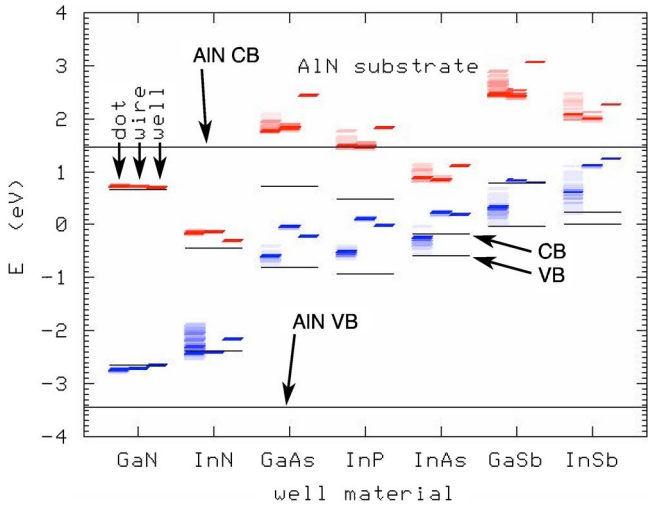

FIG. 3. (Color online) Band energies vs composition for dot, wire, and well structures on an AlN substrate. (All nitrides are zinc blende.) The two long lines spanning the graph indicate the conduction and valence band energies for the unstrained substrate material. The lines of medium length indicate the unstrained valence and conduction energies for different well materials. The short lines are histograms of the valence and conduction energies for dots, wires, and wells of the indicated composition with strain effects included. The shading of the short lines is proportional to the volume of material with the indicated energy (see Fig. 1). Energies are calculated for $k=0$ using the local value of the strain, and the histograms include all points in the well material.

proximation. Even for nanometer scale structures the effective potential obtained from the local band edge provide a useful estimate of electronic energies.[5]

Since the equations governing the strain are scale invariant, the strain and band energies do not vary with the size of the structure, and the band-edge results are applicable to any size structure. However, the size of the structure does affect the confinement energy. To facilitate estimation of the confinement energy, we have calculated mean effective masses for the structures. These were determined by numerically computing $E(\mathbf{k})$ at $\mathbf{k}=0,\pm\delta\mathbf{k}$ and fitting $E(\mathbf{k})=\hbar^2\mathbf{k}^2/2m^*$ with $|\delta\mathbf{k}|$ equal to 10^{-2} of the Brillouin zone. Anisotropy was accounted for by taking $\delta\mathbf{k}$ in the x-, y-, and z directions and averaging over those directions with confinement. Finally, the mean masses were determined by averaging over all points in the well material.

Given the dimensions of a nanostructure, the barrier height, and an effective mass one can estimate the confinement energy using a simple effective mass model. Figure 2 gives the confinement energies for quantum wells, circular wires, and spheres with various barrier heights, effective masses, and sizes. The confinement energies shown in Fig. 2 assume that the well and barrier materials have the same effective mass. For strong confinement, the penetration of the wave function into the barrier will be small, and the confinement energy will be dominated by the effective mass in the well material. For weak confinement the approximation of a uniform effective mass will be less accurate since the different effective mass in the barrier will influence the confinement energy somewhat. However, the size of this effect may be estimated by using an effective mass intermediate between that of the barrier and well.

Self-assembled quantum dots have complex and variable shapes, but we have found that modeling them as circular cylinders works well for estimating the confinement energy. Assuming a dot to be a lens-shaped cap with base diameter d and height h we model it as a circular cylinder of diameter d and a height h_{cyl} that gives the cylinder the same volume as the lens-shaped cap $[V=\pi h(2d^2+4h^2)/24]$. Since typically $h \ll d$, the confinement energy is dominated by the one-dimensional (1D) confinement along the shorter direction.

III. BINARY MATERIALS

We first consider dots, wires, and wells consisting of combinations of binary materials. For each substrate material we have plotted the conduction and valence energies of the embedded material, along with the value for the unstrained bulk substrate material. The energy of the top of the valence band for unstrained InSb has been taken as a reference level and set to zero. The spatial variation of the band edges in dots and wires is displayed as a histogram in which the shading of the lines is proportional to the frequency of a particular energy. The histograms include every point in the well material. An example of the potential profile in a quantum dot along with the corresponding histogram is shown in Fig. 1. The range of energies is larger for dots than wires as a consequence of the larger strain inhomogeneity in dots. The spatially averaged mean values of the band energies are given in Tables I–III.

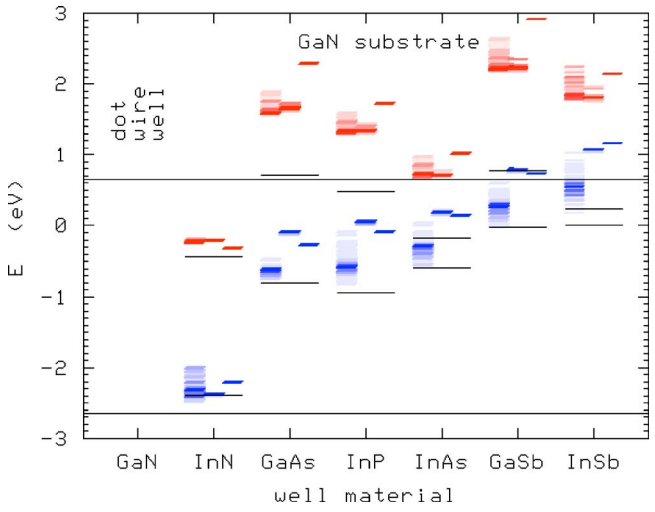

FIG. 4. (Color online) Band edge diagram of strained dots, wires, and wells on GaN. All nitrides are zinc blende (see Fig. 3 for details).

A. AlN, GaN, and InN substrates

Figures 3–5 show the energies for zinc-blende GaN, InN, GaAs, InP, InAs, GaSb, and InSb strained to AlN, GaN, and InN, respectively. We find that for AlN substrates all of the nitrides are type I, while all of the non-nitrides except InAs are type II, with only hole confinement. On GaN substrates we find only InN to be type I (i.e., confining both electrons and holes). For GaSb and InSb wires and wells there is a broken gap, with the valence maximum above the conduction minimum of GaN. In such a case the strained material will donate electrons to the barrier material. A sheet of InSb in GaN would act as a delta-doping layer. On InN substrates we find that the strained structures are either type II or have a broken gap. Common to all these cases is that the compressive strain opens up the band gap and that the top of the valence band moves up in energy compared with the unstrained situation both for compressive and tensile strain.

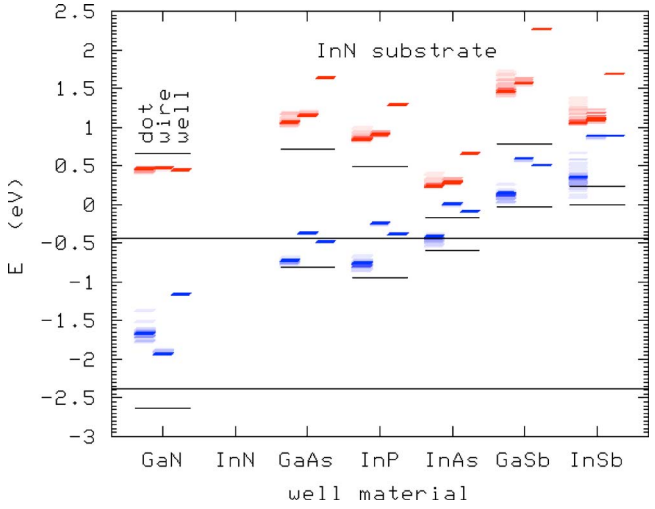

FIG. 5. (Color online) Band edge diagram of strained dots, wires, and wells on InN (see Fig. 3 for details).

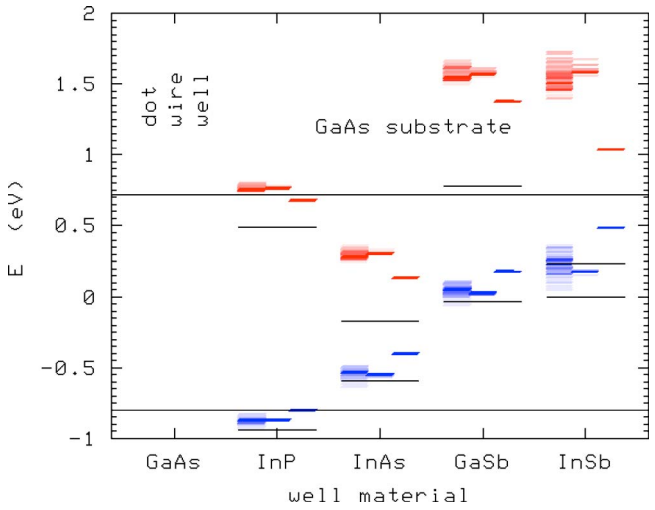

FIG. 6. (Color online) Band edge diagram of strained dots, wires, and wells on GaAs (see Fig. 3 for details).

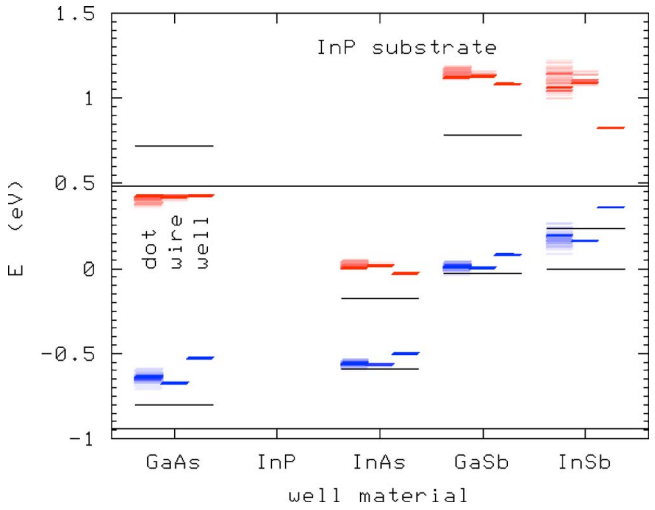

FIG. 7. (Color online) Band edge diagram of strained dots, wires, and wells on InP (see Fig. 3 for details).

Also, the spread in energies increases with increasing strain.

B. GaAs substrate

Figure 6 shows the energies for InP, InAs, GaSb, and InSb strained to GaAs, one of the most commonly used substrates. We find that the band edges of InP structures are nearly aligned with GaAs, with only small differences between InP wells, wires, and dots. For materials with greater mismatch to GaAs than InP we find that wires and dots have similar band-edge profiles, but the gaps for wells are substantially smaller. This is generally true for all non-nitride systems in which the mismatch is not too large. The reason is simply that wells can relax freely in the growth direction, resulting in a lower hydrostatic strain than for wires and dots. For sufficiently strained systems there is a strong interaction between the valence band and the conduction band allowing quantum wells to have a larger band gap than dots. For InAs dots we find an edge-to-edge gap of about 0.9 eV in agreement with previous calculations.[5,10] GaSb and InSb are both strongly type II for all geometries.

Experiments on GaSb dots in GaAs show strong photoluminescence (PL) with a gap of $E_g \approx 1.1$ eV,[11,12] and pump power dependence indicating a type II structure with hole confinement. Our calculations also indicate a type II structure with hole confinement. Measurements of uncapped GaSb/GaAs dots show them to have a diameter $d=28$ nm with a height $h=3.3$ nm.[11] To estimate the confinement energy, we approximate these dots as cylinders with the same diameter and total volume as a lens-shaped cap of the measured dimensions ($d=28$ nm and $h_{cyl}=1.68$ nm). Using the spatially averaged hole effective mass for a GaSb/GaAs dot from Table VI ($m_{eff}=0.097$) and a barrier height of 0.84 eV, the confinement energy for the growth direction is 380 meV, and the confinement energy for the transverse direction is 10 meV. Adding the confinement energy to the (spatially averaged) edge-to-edge gap gives $E_g=1.06$ eV, in excellent agreement with the measured value 1.1 eV.

InSb structures on GaAs are similar to GaSb on GaAs, with type II alignment and hole confinement for wells, wires, and dots. The calculated gaps are smaller however. PL experiments on InSb dots in GaAs indicate $E_g \approx 1.1$ eV,[11] while our estimate of the confinement energy (using $h=5.1$ nm, $d=67$ nm) gives $E_g=0.88$ eV. This discrepancy suggests that some alloying of the dot material has occurred or the covered dots are substantially smaller than measurements on uncovered dots indicate. It is likely that the dots became smaller during capping since the GaAs was deposited using migration enhanced epitaxy.[11]

C. InP substrate

Figure 7 shows the energies for materials strained to InP. On InP substrates we find that GaAs should be a type I quantum well with a band gap of about 1 eV. Experiments on 1.8 nm and 2.8 nm GaAs quantum wells on InP find a transition energy of 1.148 and 1.088 eV, respectively.[13] Our calculations of confinement energy give transition energies of 1.234 eV and 1.150 eV. It should be noted that the GaAs thicknesses are somewhat uncertain since they were determined from the growth, and were not directly measured.[13] Also, in Ref. 13 the quantum wells were interpreted using calculations with type II alignment and hole confinement. Our calculated band alignment in Fig. 7 is nearly type II, with only a 60 meV barrier for the electrons. This discrepancy in band alignments is due to different material parameters.

InAs dots in InP have been shown to be type I and to emit light at an energy of about 0.8 eV.[14] The size of the dots in Ref. 14 was determined by fitting the experimental data to detailed eight-band $\mathbf{k}\cdot\mathbf{p}$ calculations, giving dimensions of 45 nm $\times$ 35 nm $\times$ 6 nm. The confinement energy is dominated by the 6 nm dot height, and we obtain an estimated gap of $E_g=0.8$, in excellent agreement with experiment and detailed eight-band calculations.[14] (The confinement energy associated with the long dimensions of the dot is an order of magnitude smaller than that coming from the dot height.)

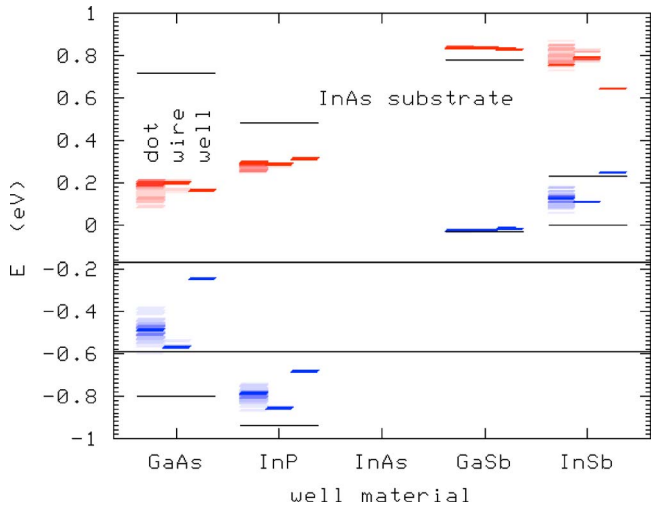

FIG. 8. (Color online) Band edge diagram of strained dots, wires, and wells on InAs (see Fig. 3 for details).

InSb quantum dots grown on InP have been found to emit photons with an energy of about 1 eV and were interpreted to have a type II band alignment.[15] This type II alignment has been confirmed by photoreflectance measurements on InSb islands which have been partially covered by InP giving a type I to type II transition with increasing cap layer thickness.[16] The dots in Ref. 15, were found to be 24±4 nm in diameter, and 6±3 nm high, as measured by AFM on uncapped dots. From these dimensions we obtain a confinement energy of 0.34 eV, giving a total gap of E_g=0.6 eV. The discrepancy between calculated and measured gaps indicates that the dots probably shrunk during deposition of the InP cap layer.

D. InAs substrate

Figure 8 shows the energies for materials strained to InAs. On InAs, only GaAs has any confinement (type II hole confinement). On InAs substrates both GaSb and InSb are expected to have broken gaps, with the valence band edge of GaSb and InSb above the conduction band minimum of InAs. This has been observed and has many interesting consequences for the electronic structure due to charge transfer. While broken gap superlattices have been studied,[17–20] lower dimensional broken gap structures remain unexplored.

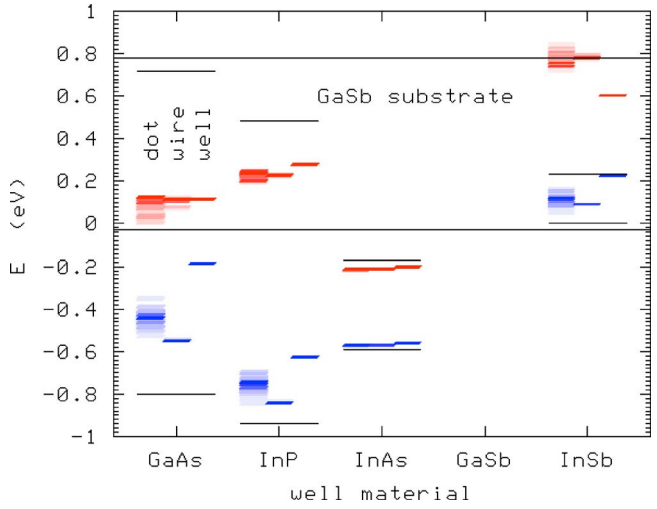

FIG. 9. (Color online) Band edge diagram of strained dots, wires, and wells on GaSb (see Fig. 3 for details).

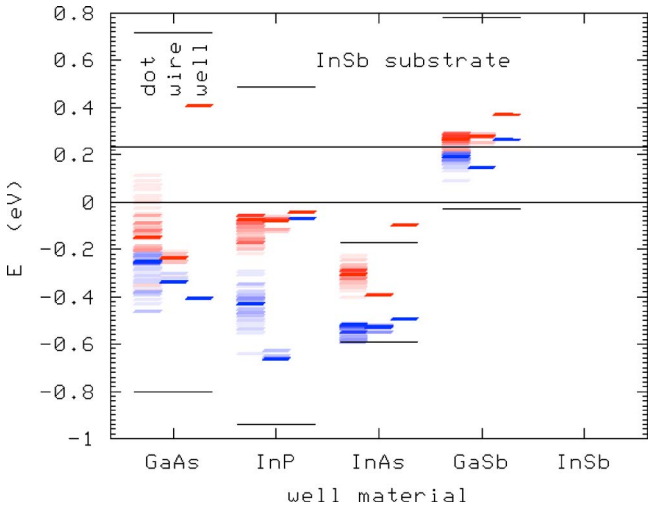

FIG. 10. (Color online) Band edge diagram of strained dots, wires, and wells on InSb (see Fig. 3 for details). For all well materials the gaps are negative, with the state containing mostly valence character being higher in energy.

E. GaSb and InSb substrates

Figures 9 and 10 shows the energies for materials strained to GaSb and InSb, respectively. Very little experimental work has been done on these substrates. However, GaSb has a very similar lattice constant to InAs and the band edges of strained structures are thus very similar on these two substrates. The band alignment is very different though and we note as an example that thin layers of InAs will donate holes to GaSb.

InSb has the interesting feature that all materials strained to it have negative gaps. For wires and wells this inversion of the conduction and valence bands should give rise to a semi-

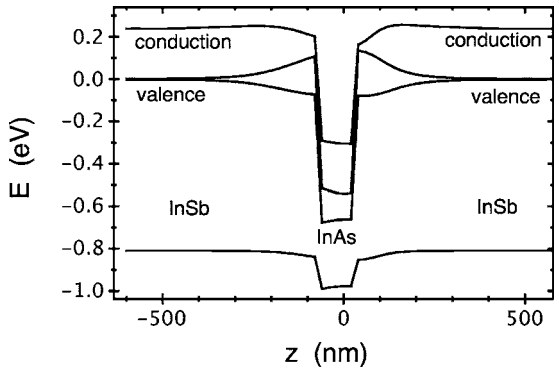

FIG. 11. Band diagram of an InAs/InSb dot along the [001] direction through the center of the dot. Electrons are strongly confined in the InAs dot, while holes see a strain induced potential well in the InSb barrier adjacent to the dot.

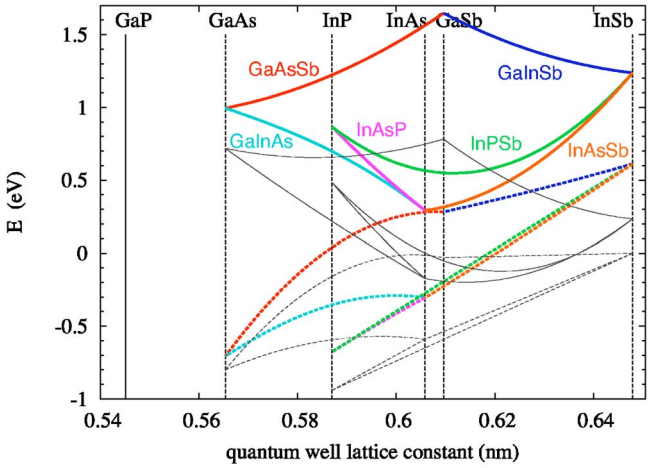

FIG. 12. (Color online) Band edge diagram of alloyed strained wells on GaP. The x axis is the lattice constant of the ternary alloy comprising the quantum well. Dotted lines are the valence band energies, solid lines are the conduction band energies, and the lighter lines are the energies for unstrained materials.

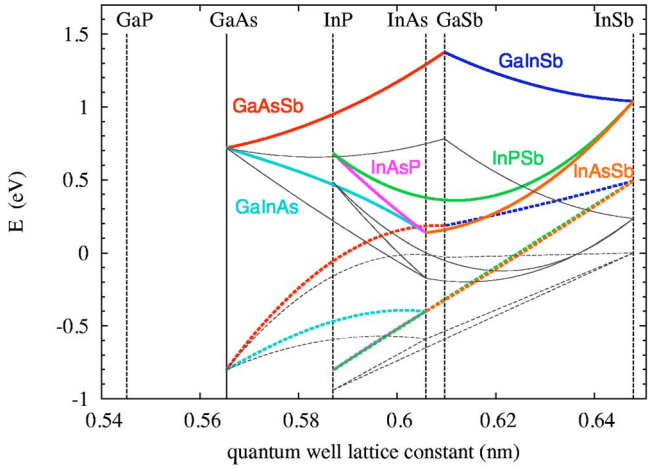

FIG. 13. (Color online) Band edge diagram of alloyed strained wells on GaAs.

metallic structure. For dots there will still be discrete confined states, however the valence and conduction Bloch states will be more mixed than usual.

F. Broken gap structures

For wires and dots the strain extends into the barrier material, affecting the electronic structure of the barrier as well. Figure 11 shows an InAs dot strained to InSb, in which the InSb barrier experiences a sufficiently strong strain that the band gap is substantially reduced near the dot. Due to the broken gap structure the InAs acts as an "artificial acceptor," but the holes see a confining potential from the InSb around the InAs dot. This results in a charged shell structure in which the InAs artificial acceptor has a negative charge which is surrounded by a positive charge bound to the strained InSb. For stacks of such dots, one would obtain semimetallic wires in which the core contains electrons, and the surrounding shell contains holes.

TABLE I. Conduction and valence band energies (in eV) for quantum wells strained to substrates of binary materials.

	Well material						
Substrate	GaN	InN	GaAs	InP	InAs	GaSb	InSb
			Conduction				
AlN	0.713	−0.292	2.452	1.840	1.112	3.082	2.279
GaN	0.659	−0.322	2.288	1.731	1.020	2.921	2.162
InN	0.444	−0.440	1.635	1.294	0.653	2.278	1.695
GaAs			0.719	0.682	0.137	1.375	1.039
InP			0.424	0.485	−0.029	1.085	0.829
InAs			0.168	0.313	−0.173	0.832	0.645
GaSb			0.117	0.279	−0.202	0.782	0.608
InSb			0.409	−0.042	−0.099	0.370	0.235
			Valence				
AlN	−2.644	−2.162	−0.212	−0.005	0.198	0.800	1.249
GaN	−2.640	−2.206	−0.268	−0.080	0.141	0.742	1.178
InN	−1.160	−2.380	−0.489	−0.381	−0.084	0.510	0.892
GaAs			−0.800	−0.804	−0.400	0.184	0.491
InP			−0.528	−0.940	−0.501	0.079	0.363
InAs			−0.246	−0.682	−0.590	−0.012	0.251
GaSb			−0.188	−0.625	−0.558	−0.030	0.228
InSb			−0.405	−0.070	−0.495	0.268	0.000

TABLE II. Mean conduction and valence band energies (in eV) for wires strained to substrates of binary materials.

	Wire material						
Substrate	GaN	InN	GaAs	InP	InAs	GaSb	InSb
			Conduction				
AlN	0.731	−0.128	1.831	1.481	0.854	2.464	2.037
GaN	0.659	−0.205	1.678	1.349	0.725	2.265	1.832
InN	0.465	−0.440	1.168	0.912	0.294	1.590	1.128
GaAs			0.719	0.769	0.309	1.581	1.600
InP			0.419	0.485	0.020	1.137	1.109
InAs			0.198	0.289	−0.173	0.837	0.795
GaSb			0.105	0.230	−0.212	0.782	0.786
InSb			−0.237	−0.082	−0.391	0.275	0.235
			Valence				
AlN	−2.712	−2.404	−0.037	0.116	0.228	0.837	1.121
GaN	−2.640	−2.377	−0.096	0.051	0.194	0.796	1.081
InN	−1.900	−2.380	−0.372	−0.250	0.009	0.591	0.886
GaAs			−0.800	−0.867	−0.554	0.025	0.182
InP			−0.676	−0.940	−0.567	0.007	0.161
InAs			−0.568	−0.852	−0.590	−0.024	0.114
GaSb			−0.544	−0.835	−0.572	−0.030	0.092
InSb			−0.330	−0.644	−0.531	0.148	0.000

TABLE III. Mean conduction and valence band energies (in eV) for dots strained to substrates of binary materials.

	Dot material						
Substrate	GaN	InN	GaAs	InP	InAs	GaSb	InSb
			Conduction				
AlN	0.733	−0.142	1.849	1.553	0.938	2.560	2.186
GaN	0.659	−0.214	1.660	1.391	0.783	2.315	1.948
InN	0.448	−0.440	1.079	0.878	0.279	1.511	1.139
GaAs			0.719	0.768	0.300	1.578	1.551
InP			0.405	0.485	0.023	1.146	1.103
InAs			0.169	0.281	−0.173	0.839	0.800
GaSb			0.078	0.224	−0.212	0.782	0.780
InSb			−0.155	−0.114	−0.307	0.256	0.235
			Valence				
AlN	−2.744	−2.253	−0.613	−0.511	−0.290	0.292	0.621
GaN	−2.640	−2.270	−0.639	−0.566	−0.321	0.257	0.563
InN	−1.658	−2.380	−0.732	−0.761	−0.441	0.124	0.337
GaAs			−0.800	−0.876	−0.542	0.042	0.232
InP			−0.641	−0.940	−0.563	0.010	0.180
InAs			−0.490	−0.794	−0.590	−0.023	0.127
GaSb			−0.443	−0.756	−0.568	−0.030	0.114
InSb			−0.300	−0.439	−0.547	0.185	0.000

TABLE IV. Mean effective masses of electrons and holes for strained quantum wells on different substrates. Values in italics are experimental electron effective masses for bulk materials. The calculated values differ because the eight-band model does not include the effects of remote bands. Since strain splits the heavy-hole–light-hole degeneracy, the hole masses are for the doubly degenerate highest valence state. Hole masses for unstrained systems are excluded because of the ambiguities due to the heavy-hole–light-hole degeneracy.

	Well material						
Substrate	GaN	InN	GaAs	InP	InAs	GaSb	InSb
				Electrons			
AlN	0.120	0.074	0.088	0.088	0.051	0.084	0.054
GaN	0.117	0.074	0.086	0.088	0.050	0.082	0.053
	0.15						
InN	0.091	0.072	0.075	0.084	0.045	0.072	0.048
		0.12					
GaAs			0.053	0.073	0.034	0.053	0.037
			0.067				
InP			0.042	0.066	0.029	0.045	0.032
				0.080			
InAs			0.028	0.058	0.023	0.036	0.028
					0.026		
GaSb			0.024	0.055	0.021	0.035	0.027
						0.039	
				Holes			
AlN	0.390	0.233	0.164	0.181	0.063	0.096	0.039
GaN		0.244	0.164	0.183	0.063	0.096	0.039
InN	0.267		0.159	0.192	0.061	0.092	0.038
GaAs				0.207	0.057	0.083	0.035
InP			0.118		0.137	0.078	0.034
InAs			0.074	0.194		0.074	0.032
GaSb			0.061	0.183	0.080		0.032

IV. EFFECTIVE MASSES

Confinement effects will increase band gaps over the results obtained above. It is simply impossible to cover all sizes and cases, so we have instead calculated the effective masses for electrons and holes, which can then be used to estimate the confinement energy. Such single-band calculations can be quite accurate, especially for quantum wells. Even for quantum dots a single band approximation using a strain-dependent effective mass gives good estimates of the gap.[5] In addition to the effective mass, the confinement energy will be effected by the geometry. However, the confinement energy is primarily determined by the smallest dimension of the dot, with the detailed shape playing a smaller role.[9]

The results are summarized in Tables IV–VI which give the mean effective masses, spatially averaged over the well material, and over directions in which there is confinement (see Sec. III). Since the heavy-hole light-hole degeneracy is split by strain the hole effective masses are those for the highest valence state, which is a mixture of heavy and light holes, but is primarily heavy hole.

Results for InSb substrates were omitted because all well materials have negative gaps (i.e., strain causes the state with primarily valence character to be higher than the conduction state.) Nitride materials on non-nitride substrates were also omitted because of the extremely large range of effective masses throughout the well material (see Tables IV–VI). When nitrides are considered, they are assumed to be in the zinc-blende form.

Table IV (for quantum wells) includes both the calculated and experimental electron effective masses, which differ because the eight-band model does not include the effects of remote bands. The effective electron mass is given by

$$m^* = m_0 \left[(1+2F) + \frac{E_P(E_g + 2\Delta/3)}{E_g(E_g+\Delta)} \right]^{-1}, \tag{1}$$

$$F = \frac{1}{m_0} \sum_r \frac{|\langle S|p_x|u_r\rangle|^2}{E_c - E_r}, \tag{2}$$

where E_g is the gap, Δ is the spin-orbit coupling, E_P is the Kane matrix element, and F is the Kane parameter for the

TABLE V. Mean effective masses of electrons and holes for strained quantum wires on different substrates.

	Wire material						
Substrate	GaN	InN	GaAs	InP	InAs	GaSb	InSb
			Electrons				
AlN	0.122	0.082	0.078	0.088	0.051	0.076	0.062
GaN	0.117	0.080	0.075	0.085	0.046	0.071	0.055
InN	0.099	0.072	0.064	0.075	0.031	0.055	0.028
GaAs			0.053	0.076	0.045	0.061	0.065
InP			0.043	0.066	0.032	0.047	0.049
InAs			0.034	0.058	0.023	0.037	0.039
GaSb			0.031	0.055	0.020	0.035	0.039
			Holes				
AlN	0.456	0.354	0.155	0.193	0.082	0.101	0.059
GaN		0.353	0.154	0.191	0.077	0.098	0.056
InN	0.414		0.152	0.194	0.059	0.086	0.036
GaAs				0.254	0.084	0.100	0.053
InP			0.115		0.064	0.085	0.047
InAs			0.088	0.184		0.071	0.041
GaSb			0.078	0.178	0.046		0.040

TABLE VI. Mean effective masses of electrons and holes for strained quantum dots on different substrates.

	Dot material						
Substrate	GaN	InN	GaAs	InP	InAs	GaSb	InSb
			Electrons				
AlN	0.121	0.080	0.082	0.095	0.062	0.082	0.072
GaN	0.117	0.078	0.077	0.092	0.057	0.077	0.066
InN	0.097	0.072	0.063	0.078	0.041	0.057	0.045
GaAs			0.053	0.076	0.044	0.060	0.061
InP			0.042	0.066	0.032	0.047	0.047
InAs			0.032	0.057	0.023	0.036	0.037
GaSb			0.028	0.054	0.020	0.035	0.036
			Holes				
AlN	0.441	0.534	0.189	0.275	0.085	0.110	0.049
GaN		0.539	0.183	0.269	0.082	0.106	0.048
InN	0.343		0.162	0.239	0.068	0.092	0.042
GaAs				0.237	0.074	0.097	0.048
InP			0.124		0.063	0.085	0.044
InAs			0.097	0.211		0.075	0.040
GaSb			0.085	0.202	0.043		0.040

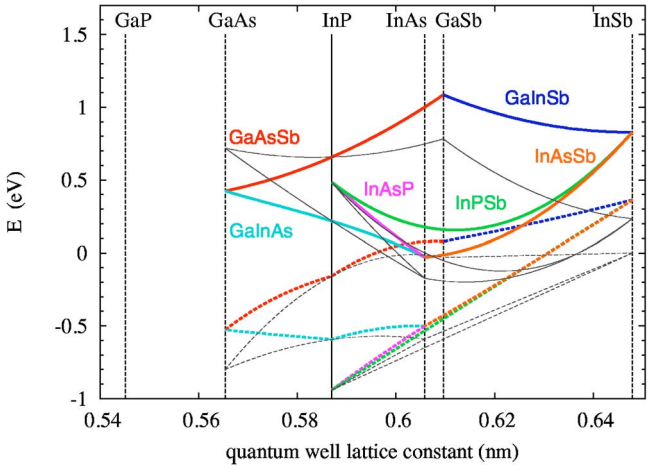

FIG. 14. (Color online) Band edge diagram of alloyed strained wells on InP.

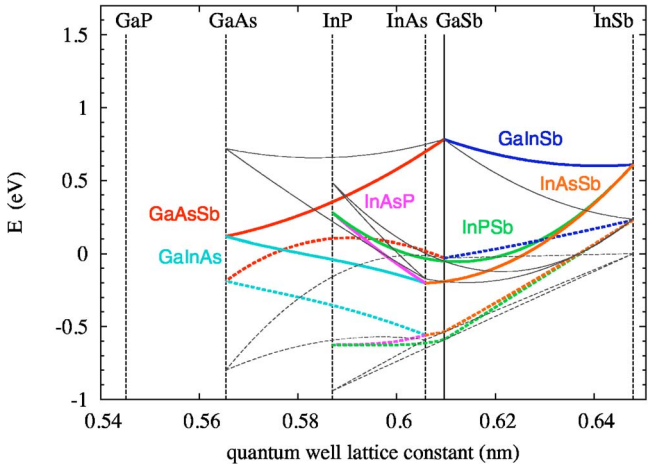

FIG. 16. (Color online) Band edge diagram of alloyed strained wells on GaSb.

effects of remote bands, where the index r goes over the remote bands. For most of the materials, the eight-band effective mass differs from the experimental value by 10–20%, which is smaller than the variation in the effective mass due to strain inhomogeneities.[5]

V. TERNARY SLABS

We now turn to quantum wells composed of ternary alloys on substrates with different lattice constants. We have calculated the band edges of the ternary alloys interpolating among GaAs, InP, InAs, GaSb, and InSb, when strained to substrates with increasing lattice constants ranging from that of GaP to InSb. Figures 12–17 show the band edges of the alloys strained to binary substrates (GaAs, InP, InAs, GaSb, and InSb). The complete results including substrates with intermediate lattice constants are available electronically.[21]

As expected, the conduction band edges increase in energy when subjected to compressive strain. In contrast, the valence band edges increase in energy for both compressive and tensile strain. This behavior is due to the degeneracy of the states at the top of the valence band. In the absence of strain the top of the valence band consists of degenerate heavy and light hole states which are insensitive to hydrostatic strain, but split under biaxial strain. Since this splitting raises one band and lowers the other, the valence band edge increases regardless of the sign of the biaxial strain.

For sufficiently large substrate lattice constants the well's material gap may become very small and even negative (e.g., GaAs on InSb). We note that for substrate lattice constants >0.62 nm we begin to see negative band gaps, which could be useful for small-band-gap applications. Substrates with almost arbitrary lattice constants may be obtained using flexible substrates.[22] Such structures could also be obtained from free-standing wires (whiskers) with properly selected alloy composition.

A well material that is nominally metallic due to strain may obtain a gap due to confinement. It may thus be possible to obtain narrow gap quantum wells, provided the well thickness can be made sufficiently large that the confinement energy is not too large. With increasing lattice mismatch the bandgap of the well material decreases, but the quantum well thickness decreases as well,[3] thus increasing the confinement

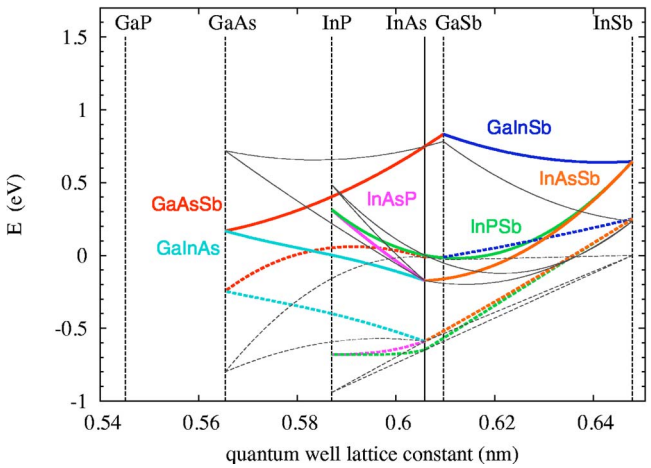

FIG. 15. (Color online) Band edge diagram of alloyed strained wells on InAs.

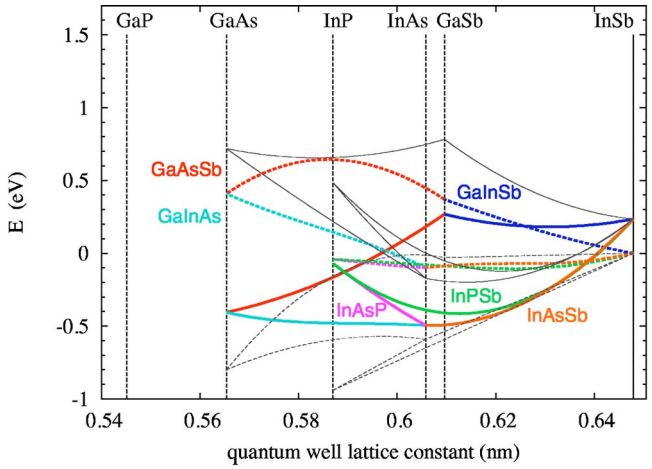

FIG. 17. (Color online) Band edge diagram of alloyed strained wells on InSb.

energy. Therefore, designing a narrow gap quantum well requires tradeoffs between the band gap of the strained material and the thickness of the quantum well.

VI. SUMMARY

We have calculated band edges for strained quantum wells, circular wires, and lens-shaped dots for a large set of III-V compounds, including alloys. We have also calculated the effective masses which can be used as inputs for further single band calculations to obtain the electronic structure when the absolute size of the structures is known. These diagrams are useful for identifying material combinations with desired band offsets. We have also identified material combinations for which the embedded materials behave as artificial donors or acceptors.

ACKNOWLEDGMENTS

We thank N. Panev, M. K.-J. Johansson, J. Persson, and M. Miller for critical reading and enlightening comments. This work was performed within the nanometer structure consortium in Lund and supported by the Swedish Foundation for Strategic Research (SSF), the Swedish Research Council (VR), and in part by the European Community's Human Potential Program under Contract No. HPRN-CT-2002-00298, (Photon Mediated Phenomena).

*Electronic address: craig-pryor@uiowa.edu
†Electronic address: mats-erik.pistol@ftf.lth.se

[1] S. Tiwari and D. J. Frank, Appl. Phys. Lett. **60**, 630 (1992).
[2] M. T. Björk, B. J. Ohlsson, T. Sass, A. I. Persson, C. Thelander, M. H. Magnusson, K. Deppert, L. R. Wallenberg, and L. Samuelson, Appl. Phys. Lett. **80**, 1058 (2002).
[3] J. W. Matthews and A. E. Blakeslee, J. Cryst. Growth **27**, 118 (1974).
[4] C. Pryor, M.-E. Pistol, and L. Samuelson, Phys. Rev. B **56**, 10404 (1997).
[5] C. Pryor, Phys. Rev. B **57**, 7190 (1998), cond-mat/9710304.
[6] T. B. Bahder, Phys. Rev. B **41**, 11 992 (1990).
[7] I. Vurgaftman, J. R. Meyer, and L. R. Ram-Mohan, J. Appl. Phys. **89**, 5815 (2001).
[8] T. Matsuoka, H. Okamoto, M. Nakao, H. Harima, and E. Kurimoto, Appl. Phys. Lett. **81**, 1246 (2002).
[9] C. Pryor, Phys. Rev. B **60**, 2869 (1999).
[10] O. Stier, M. Grundmann, and D. Bimberg, Phys. Rev. B **59**, 5688 (1999).
[11] B. R. Bennett, P. M. Thibado, M. E. Twigg, E. R. Glaser, R. Magno, B. V. Shanabrook, and L. J. Whitman, J. Vac. Sci. Technol. B **14**, 2195 (1996).
[12] F. Hatami *et al.*, Appl. Phys. Lett. **67**, 656 (1995).
[13] M.-E. Pistol, M. Gerling, D. Hessman, and L. Samuelson, Phys. Rev. B **45**, 3628 (1992).
[14] H. Pettersson, C. Pryor, L. Landin, M.-E. Pistol, N. Carlsson, W. Seifert, and L. Samuelson, Phys. Rev. B **61**, 4795 (2000).
[15] T. Utzmeier, J. Tamayo, P. A. Postigo, R. Garcia, and F. Briones, J. Chem. Phys. **175**, 725 (1997).
[16] J. A. Prieto, G. Armelles, T. Utzmeier, F. Briones, J. C. Ferrer, F. Peiro, A. Cornet, and J. R. Morante, Phys. Rev. Lett. **80**, 1094 (1998).
[17] L. L. Chang, N. Kawai, G. A. Sai-Halasz, R. Ludeke, and L. Esaki, Appl. Phys. Lett. **35**, 939 (1979).
[18] M. Altarelli, Phys. Rev. B **28**, 842 (1983).
[19] A. Krier, X. L. Huang, and A. Hammiche, Appl. Phys. Lett. **77**, 3791 (2000).
[20] J. H. Roslund, K. Saito, K. Suzuki, H. Yamaguchi, and Y. Hirayama, Jpn. J. Appl. Phys., Part 1 **39**, 2448 (2000).
[21] C. E. Pryor and M.-E. Pistol cond-mat/0501090, Phys Rev. B (to be published).
[22] K. Eisenbeiser, R. Emrick, R. Droopad, Z. Yu, J. Finder, S. Rockwell, J. Holmes, C. Overgaard, and W. Ooms, IEEE Electron Device Lett. **23**, 300 (2002).